Load Transfer Analysis in Short Carbon Fibers with Radially-Aligned Carbon Nanotubes Embedded in a Polymer Matrix

M. C. Ray
Department of Mechanical Engineering, Indian Institute of Technology, Kharagpur 721302, India

Roberto Guzman de Villoria and Brian L. Wardle
Department of Aeronautics and Astronautics, Massachusetts Institute of Technology, Cambridge, MA 02139, USA

A novel shortfiber composite in which the microscopic advanced fiber reinforcements are coated with radially aligned carbon nanotubes (**CNT**s) is analyzed in this study. A shear-lag model is developed to analyze the load transferred to such coated fibers from the aligned-**CNT** reinforced matrix in a hybrid composite application. It is found that if the carbon fibers are coated with radially aligned **CNT**s, then the axial load transferred to the fiber is reduced due to stiffening of the matrix by the **CNT**s. Importantly, it is shown that at low loading of **CNT**s in the polymer matrix, there is a significant reduction in the maximum interfacial shear stress, e.g., at 1% **CNT**s, there is an ~25 % reduction in this maximum stress. Further, the modification in the load sharing between the fiber and the matrix plateaus at ~2% **CNT** matrix loading, indicating a small but critical window for engineering the interface in this manner. Effects of the variation of the aspect ratio of the fiber, **CNT** volume fraction and the application of radial load on the load transferred to such **CNT** coated fibers are also investigated.

KEYWORDS: Nanocomposites, Composite Structures

1. Introduction

The identification of carbon nanotubes[1] (**CNT**s) has stimulated extensive research devoted to the prediction of their elastic properties through experiments and theoretical modeling. Of interest is to determine elastic properties of the **CNT**s as an input to models that predict composite behaviour. Early work by Treacy et al.[2] experimentally determined that **CNT**s have Young's modulus in the terapascal (**TPa**) range. Li and Chou[3] linked structural and molecular mechanics (**MM**) approaches to compute elastic properties of **CNT**s. Sears and Batra[4] used three **MM** potentials to simulate axial and torsional deformations of a **CNT** assuming that the tube can be regarded as a hollow cylinder of mean diameter equal to that of the **CNT** and determined the wall thickness, Young's modulus and Poisson's ratio of the **CNT**. Shen and Li[5] assumed that a **CNT** should be modeled as a transversely isotropic material with the axis of transverse isotropy coincident with the centroidal axis of the tube. They determined values of the five elastic constants by using a **MM** potential and an energy equivalence principle. Batra and Sears[6] proposed that the axis of transverse isotropy of a **CNT** is a radial line rather than the centroidal axis of the tube and found that Young's modulus in the radial direction equals about $1/4^{th}$ of that in the axial direction. Wu et al.[7] developed an atomistic based finite deformation shell theory for single-walled **CNT** and found its stiffness in tension, bending and torsion.

A great deal of research has also been carried out on the prediction of effective elastic properties of **CNT**-reinforced composites. For example, Thostensen and Chou[8] have estimated the elastic moduli of **CNT**-reinforced composite through micromechanical analysis. Gao and Li[9] derived a shear lag model of **CNT** reinforced

polymer composites by replacing the **CNT** with an equivalent solid fiber. Song and Yoon[10] numerically estimated the effective elastic properties of **CNT**-reinforced polymer based composites. Siedel and Lagoudas[11] carried out a micromechanical analysis to estimate the effective properties of **CNT**-reinforced composites. Guzman de Villoria and Miravete devolped a model to estimate the effect of the CNTs dispersion in composites matrix by micromechanical analysis[12]. Jiang et al.[13] derived a continuum based model to study the effect of **CNT**/matrix interface on the macroscopic properties of **CNT**-reinforced composites. Odegard et al.[14, 15] have modeled **CNT**-reinforced composite to estimate effective elastic moduli using an equivalent-continumm modeling method that connects computational chemistry and solid mechanics models. To avoid the long times of simulation of materials at nanoscale level, Yamakov and Glaessgen[16] have linked continuum mechanics in with atomic-level simulations, in one case to study the fracture tip of several metals. Zhang and He[17] theoretically investigated the viscoelastic behavior of **CNT**-reinforced composites developing a three-phase shear-lag model. Most recently, Ray and Batra[18] carried out a micromechanical analysis to estimate the effective elastic and piezoelectric properties of **CNT** and piezoelectric fiber reinforced hybrid composite. Several review articles have appeared that summarize the various advances in these two-phase (**CNT**s plus a matrix) nanocomposites[19-21].

Here we analyze a new hybrid composite composed of micron-scale diameter advanced fibers with *in situ* grown radially aligned **CNT**s and a polymer matrix. Growth of aligned **CNT**s on advanced fibers (see examples in Figure 1) have been investigated by several groups[22-26] and recently, bulk composites have been realized using aligned 'fuzzy' fibers[27-29]. The objective of this work is to investigate the load transferred to a

carbon fiber from the matrix in the case where the micon-scale fuzzy fiber is discontinuous (see Figure 2). A closed-form shear lag model is developed for such investigation, incorporating a micromechanics model for predicting the radially-orthotropic properties of the aligned-**CNT** reinforced polymer matrix. Such composites can be described as a hybrid nano-engineered composite, where the polymer matrix is reinforced with radially aligned-**CNT** resulting in an aligned-**CNT** nanocomposite matrix that surrounds the micron-scale advanced fiber (see Figure 3). Such nano-engineered composites can be fabricated using capillarity-driven wetting of the aligned **CNT**s by advanced polymers[29, 30].

2. Shear lag model

A schematic sketch of the cylindrical representative volume element (**RVE**) of the composite analyzed here is shown in Figure 3. The cylindrical coordinate system ($\mathbf{r}$, θ and $\mathbf{x}$) is considered in such a way that the axis of the **RVE** coincides with the $\mathbf{x}$ axis while the **CNT**s are aligned along the $\mathbf{r}$-direction. The model is derived by dividing the **RVE** into three zones. The portion of the **RVE** in the zone $-\mathbf{L_f} \le \mathbf{x} \le \mathbf{L_f}$ consists of a discontinuous micro-scale advanced fiber (carbon is considered here) reinforcement on which radially aligned **CNT**s have been grown. When this resulting fuzzy fiber is embedded in a polymer material, the **CNT** forest is filled with the polymer creating a nano-reinforced polymer matrix, what many have called a polymer nanocomposite (**PNC**) [31, 32]. Thus, the radially aligned **CNT**s reinforce the polymer matrix and the portion of the **RVE** in the zone $-\mathbf{L_f} \le \mathbf{x} \le \mathbf{L_f}$ can be viewed as a hybrid composite comprised of the carbon fiber reinforcement embedded in the **CNT**-reinforced polymer

matrix composite phase. The radius and the length of the carbon fiber are denoted by $\mathbf{a}$ and $2\mathbf{L_f}$, respectively. The inner and outer radii of the **CNT**-reinforced matrix phase are $\mathbf{a}$ and $\mathbf{R}$, respectively. The portions of the **RVE** in the zones $-\mathbf{L} \le \mathbf{x} \le -\mathbf{L_f}$ and $\mathbf{L_f} \le \mathbf{x} \le \mathbf{L}$ are treated in the model as an imaginary fiber and the matrix phase, both composed of the polymer material. The radius of the imaginary fiber is also denoted by $\mathbf{a}$ while the inner and outer radii of the matrix phase are also represented by $\mathbf{a}$ and $\mathbf{R}$, respectively. Thus, the shear lag model developed for the zone $-\mathbf{L_f} \le \mathbf{x} \le \mathbf{L_f}$ can be applied to derive the shear lag models for the zones $-\mathbf{L} \le \mathbf{x} \le -\mathbf{L_f}$ and $\mathbf{L_f} \le \mathbf{x} \le \mathbf{L}$.

In what follows, the shear lag model for the zone $-\mathbf{L_f} \le \mathbf{x} \le \mathbf{L_f}$ is first derived. A tensile stress $\boldsymbol{\sigma}_0$ is applied to the **RVE** along $\mathbf{x}$ direction at $\mathbf{x} = \pm\mathbf{L}$ while the **RVE** is subjected to a *radial* normal stress $\mathbf{q}_0$ at $\mathbf{r} = \mathbf{R}$. In order to derive this shear lag model, the effective properties of the aligned **CNT**-reinforced matrix phase are needed. This **PNC** matrix phase has transverse isotropy in a radial coordinate system due to the **CNT** alignment and isotropic nature of the polymer. This is a slight approximation because the grown **CNT**s have reduced volume fraction as they grow radially, but volume fraction may be considered constant over the small (microns) **CNT** lengths considered. Micromechanics is used to calculate properties in this region as they have not been determined experimentally to date. A micromechanics model by Ray and Batra[18] is used to calculate the effective elastic constants for a forest of aligned single-walled **CNT**s (properties from Ref.[5] given in Table 1) embedded in a polymer (results summarized in Table 2). These results are used as an input to the shear-lag model.

Returning to the shear-lag model, the governing equations for the different

phases of this **RVE** concerning equilibrium along $\mathbf{x}$ direction are given by

$$\frac{\partial \sigma_{\mathbf{x}}^{\mathbf{i}}}{\partial \mathbf{x}} + \frac{1}{\mathbf{r}} \frac{\partial (\mathbf{r} \sigma_{\mathbf{xr}}^{\mathbf{i}})}{\partial \mathbf{r}} = 0 \,, \; \mathbf{i} = \mathbf{f} \text{ and } \mathbf{m}$$

(1)

while the relevant constitutive relations are

$$\sigma_{\mathbf{x}}^{\mathbf{i}} = \mathbf{C}_{11}^{\mathbf{i}} \in_{\mathbf{x}}^{\mathbf{i}} + \mathbf{C}_{12}^{\mathbf{i}} \in_{\boldsymbol{\theta}}^{\mathbf{i}} + \mathbf{C}_{13}^{\mathbf{i}} \in_{\mathbf{r}}^{\mathbf{i}} \text{ and } \sigma_{\mathbf{xr}}^{\mathbf{i}} = \mathbf{C}_{55}^{\mathbf{i}} \in_{\mathbf{xr}}^{\mathbf{i}} \; ; \; \mathbf{i} = \mathbf{f} \text{ and } \mathbf{m}$$

(2)

In Eqs. (3) and (4), superscripts $\mathbf{f}$ and $\mathbf{m}$ denote, respectively, the carbon fiber and the **CNT**-reinforced **PNC** matrix. For the $\mathbf{i}$-th constituent phase, $\sigma_{\mathbf{x}}^{\mathbf{i}}$ and $\sigma_{\mathbf{r}}^{\mathbf{i}}$ represent the normal stresses in the $\mathbf{x}$ and $\mathbf{r}$, directions, respectively; $\in_{\mathbf{x}}^{\mathbf{i}}$, $\in_{\boldsymbol{\theta}}^{\mathbf{i}}$ and $\in_{\mathbf{r}}^{\mathbf{i}}$ are the normal strains along $\mathbf{x}$, θ and $\mathbf{r}$, directions, respectively; $\sigma_{\mathbf{xr}}^{\mathbf{i}}$ is the transverse shear stress, $\in_{\mathbf{xr}}^{\mathbf{i}}$ is the transverse shear strain and $\mathbf{C}_{\mathbf{ij}}^{\mathbf{i}}$ are the elastic constants . It should be noted here that the principal material coordinates 1, 2, 3 axes are also considered to be coincident with the problem coordinate axes $\mathbf{x}$, θ , $\mathbf{r}$, respectively. Hence, the conventional subscripts are used to write the elastic constants appearing in Eq. (2). The strain-displacement relations for an axisymmetric problem relevant to this **RVE** are

$$\in_{\mathbf{x}}^{\mathbf{i}} = \frac{\partial \mathbf{u}^{\mathbf{i}}}{\partial \mathbf{x}} \,, \; \in_{\boldsymbol{\theta}}^{\mathbf{i}} = \frac{\mathbf{w}^{\mathbf{i}}}{\mathbf{r}} \,, \; \in_{\mathbf{r}}^{\mathbf{i}} = \frac{\partial \mathbf{w}^{\mathbf{i}}}{\partial \mathbf{r}} \text{ and } \in_{\mathbf{xr}}^{\mathbf{i}} = \frac{\partial \mathbf{u}^{\mathbf{i}}}{\partial \mathbf{r}} + \frac{\partial \mathbf{w}^{\mathbf{i}}}{\partial \mathbf{x}} \,; \; \mathbf{i} = \mathbf{f} \text{ and } \mathbf{m}$$

(3)

in which $\mathbf{u^i}$ and $\mathbf{w^i}$ represent the axial and radial displacements at any point of the $\mathbf{i}$-th phase along $\mathbf{x}$ and $\mathbf{r}$, directions, respectively. The traction boundary conditions are given by

$$\boldsymbol{\sigma}_{\mathbf{r}}^{\mathbf{m}}\Big|_{\mathbf{r=R}} = \mathbf{q}_0 \text{ and } \boldsymbol{\sigma}_{\mathbf{xr}}^{\mathbf{m}}\Big|_{\mathbf{r=R}} = 0$$

(4)

and the continuity conditions are

$$\boldsymbol{\sigma}_{\mathbf{r}}^{\mathbf{f}}\Big|_{\mathbf{r=a}} = \boldsymbol{\sigma}_{\mathbf{r}}^{\mathbf{m}}\Big|_{\mathbf{r=a}},\ \boldsymbol{\sigma}_{\mathbf{xr}}^{\mathbf{f}}\Big|_{\mathbf{r=a}} = \boldsymbol{\sigma}_{\mathbf{xr}}^{\mathbf{m}}\Big|_{\mathbf{r=a}} = \boldsymbol{\tau}_{\mathbf{i}},\ \mathbf{u}^{\mathbf{f}}\Big|_{\mathbf{r=a}} = \mathbf{u}^{\mathbf{m}}\Big|_{\mathbf{r=a}} \text{ and } \mathbf{w}^{\mathbf{f}}\Big|_{\mathbf{r=a}} = \mathbf{w}^{\mathbf{m}}\Big|_{\mathbf{r=a}}$$

(5)

Where, $\boldsymbol{\tau}_{\mathbf{i}}$ is the transverse shear stress at the interface between the carbon fiber and the **PNC** matrix phase The average axial stresses in the different phases are defined as

$$\bar{\boldsymbol{\sigma}}_{\mathbf{x}}^{\mathbf{f}} = \frac{1}{\boldsymbol{\pi}\mathbf{a}^2}\int_0^{\mathbf{a}} \boldsymbol{\sigma}_{\mathbf{x}}^{\mathbf{f}}\, 2\boldsymbol{\pi}\mathbf{r}\mathbf{dr} \text{, and } \bar{\boldsymbol{\sigma}}_{\mathbf{x}}^{\mathbf{m}} = \frac{1}{\boldsymbol{\pi}(\mathbf{R}^2 - \mathbf{a}^2)}\int_{\mathbf{a}}^{\mathbf{R}} \boldsymbol{\sigma}_{\mathbf{x}}^{\mathbf{m}}\, 2\boldsymbol{\pi}\mathbf{r}\mathbf{dr}$$

(6)

Now, making use of Eqs. (1) and (4) to (6), it can be derived that

$$\frac{\partial \bar{\boldsymbol{\sigma}}_{\mathbf{x}}^{\mathbf{f}}}{\partial \mathbf{x}} = -\frac{2}{\mathbf{a}}\boldsymbol{\tau}_{\mathbf{i}} \text{ and } \frac{\partial \bar{\boldsymbol{\sigma}}_{\mathbf{x}}^{\mathbf{m}}}{\partial \mathbf{x}} = \frac{2\mathbf{a}}{\mathbf{R}^2 - \mathbf{a}^2}\boldsymbol{\tau}_{\mathbf{i}}$$

(7)

Since the radial dimension of this **RVE** is very small, it is reasonable to assume that the gradient of σ_x^m with respect to the axial coordinate (x) is independent of the radial coordinate (r). Thus let us assume that

$$\frac{\partial \sigma_x^m}{\partial x} = \phi(x) \tag{8}$$

Integrating the governing equation (1) for the **PNC** matrix phase from r to R, it can be shown that

$$\phi(x) = -\frac{2r}{R^2 - r^2}\sigma_{xr}^m \tag{9}$$

Substituting $\sigma_{xr}^m\Big|_{r=a} = \tau_i$ in Eq. (9), the transverse shear stress in the **PNC** matrix can be expressed in terms of the interface shear stress τ_i as follows:

$$\sigma_{xr}^m = \left(\frac{R^2}{r} - r\right)\frac{a}{(R^2 - a^2)}\tau_i \tag{10}$$

Also, since the **RVE** is an axisymmetric problem, it may further be assumed that the gradient $\frac{\partial w^i}{\partial x}$ of radial displacements with respect to x-direction is negligible and so, from the constitutive relation (2) between σ_{xr}^m and ϵ_{xr}^m one can write,

$$\frac{\partial \mathbf{u}^{\mathbf{m}}}{\partial \mathbf{x}} = \frac{1}{\mathbf{C}_{55}^{\mathbf{i}}}\boldsymbol{\sigma}_{\mathbf{rx}}^{\mathbf{m}}$$

(11)

Solving Eq. (11), the axial displacement of the matrix phase along $\mathbf{x}$ direction can be derived as follows:

$$\mathbf{u}^{\mathbf{m}} = \mathbf{u}_{\mathbf{a}}^{\mathbf{f}} + \mathbf{A}_1\boldsymbol{\tau}_{\mathbf{i}}$$

(12)

in which $\mathbf{u}_{\mathbf{a}}^{\mathbf{f}} = \mathbf{u}^{\mathbf{f}}\Big|_{\mathbf{r=a}}$ and $\mathbf{A}_2 = \frac{\mathbf{a}}{\mathbf{C}_{55}^{\mathbf{m}}(\mathbf{R}^2 - \mathbf{a}^2)}\left\{\mathbf{R}^2 \ln\frac{\mathbf{r}}{\mathbf{a}} - \frac{1}{2}(\mathbf{r}^2 - \mathbf{a}^2)\right\}$

(13)

The radial displacements in the two phases can be assumed as in[33] :

$$\mathbf{w}^{\mathbf{f}} = \mathbf{A}_{\mathbf{f}}\mathbf{r} \text{ and } \mathbf{w}^{\mathbf{m}} = \mathbf{A}_{\mathbf{m}}\mathbf{r} + \frac{\mathbf{B}_{\mathbf{m}}}{\mathbf{r}}$$

(14)

where $\mathbf{A}_{\mathbf{f}}$, $\mathbf{A}_{\mathbf{m}}$ and $\mathbf{B}_{\mathbf{m}}$ are unknown constants. Invoking the continuity conditions for radial displacement at the interface ($\mathbf{r} = \mathbf{a}$) it can be found that:

$$\mathbf{w}^{\mathbf{m}} = \frac{\mathbf{a}^2}{\mathbf{r}}\mathbf{A}_{\mathbf{f}} + (\mathbf{r} - \frac{\mathbf{a}^2}{\mathbf{r}})\mathbf{A}_{\mathbf{m}}$$

(15)

Invoking the continuity condition $\sigma_r^f\big|_{r=a} = \sigma_r^m\big|_{r=a}$ and satisfying the boundary condition $\sigma_r^m\big|_{r=R} = q_0$, the following equations for solving A_f and A_m are derived :

$$\begin{bmatrix} A_{11} & A_{12} \\ A_{21} & A_{22} \end{bmatrix} \begin{Bmatrix} A_f \\ A_m \end{Bmatrix} = \begin{Bmatrix} C_{13}^m - C_{12}^f \\ C_{13}^m \end{Bmatrix} \frac{\bar{\sigma}_x^f}{C_{11}^f} + \begin{Bmatrix} 0 \\ -1 \end{Bmatrix} q_0 + \begin{Bmatrix} 0 \\ A_2 C_{13}^m \end{Bmatrix} \frac{\partial \tau_i}{\partial x}$$

(16)

where,

$$A_{11} = C_{11}^f + C_{12}^f - \frac{2(C_{12}^f)^2}{C_{11}^f} + C_{33}^m - C_{23}^m,\ A_{12} = -2C_{33}^m,\ A_{21} = (C_{33}^m - C_{23}^m)\frac{a^2}{R^2} + \frac{2C_{13}^m C_{12}^f}{C_{11}^f},$$

$$A_{22} = C_{23}^m + C_{33}^m + (C_{33}^m - C_{23}^m)\frac{a^2}{R^2},\ A_2 = A_1\big|_{r=R}.$$

From Eq. (16), the solutions of A_f and A_m can be expressed as:

$$A_f = L_{11}\bar{\sigma}_x^f + L_{12}q + L_{13}\frac{\partial \tau_i}{\partial x} \text{ and } A_m = L_{21}\bar{\sigma}_x^f + L_{22}q + L_{23}\frac{\partial \tau_i}{\partial x}$$

(17)

The expressions of the coefficients L_{ij} are evident from Eq. (16) and are not shown here for the sake of brevity. The equilibrium of force along the axial (x) direction yields

$$\pi R^2 \sigma_0 = \int_0^a \sigma_x^f 2\pi r dr + \int_a^R \sigma_x^m 2\pi r dr$$

(18)

Using Eqs. (6), (17) and the constitutive relations, Eq. (18) can be reduced to

$$\frac{\partial \tau_i}{\partial x} = \frac{R^2 \sigma_0}{L_3} + \frac{L_1}{L_3} q_0 - \frac{L_2}{L_3} \bar{\sigma}_x^f$$

(19)

where,

$$L_1 = B_1 L_{12} - B_2 L_{22},\ L_2 = a^2 + \frac{C_{11}^m}{C_{11}^f}(R^2 - a^2) - B_1 L_{11} + B_2 L_{21},\ L_3 = A_3 C_{11}^m - B_1 L_{13} + B_2 L_{23},$$

$$A_3 = \int_a^R 2A_1 r dr,\ B_1 = 2\int_a^R \left[\frac{2C_{12}^f C_{11}^m}{C_{11}^f} r - (C_{12}^m - C_{13}^m)\frac{a^2}{r} \right] dr,$$

and $$B_2 = 2\int_a^R \left[(C_{12}^m + C_{13}^m) r - (C_{12}^m - C_{13}^m)\frac{a^2}{r} \right] dr.$$

Substitution of Eq. $(7)_1$ into Eq. (19) yields the governing equation for the average axial stress in the carbon fiber coated with radially aligned **CNT**s as follows:

$$\frac{\partial^2 \bar{\sigma}_x^f}{\partial x^2} - \alpha^2 \bar{\sigma}_x^f = -\eta \sigma_0 - \mu q_0$$

(20)

where,

$$\alpha^2 = \frac{2L_2}{aL_3},\ \eta = \frac{2R^2}{aL_3} \text{ and } \mu = \frac{2L_1}{aL_3}$$

(21)

Following the above procedure, the governing equation for the average axial stress ($\bar{\sigma}_x^{pf}$) in the imaginary fiber made of the polymer material lying in the zones $-L \le x \le -L_f$ and $L_f \le x \le L$ can be written as

$$\frac{\partial^2 \bar{\sigma}_x^{pf}}{\partial x^2} - \alpha_1^2 \bar{\sigma}_x^{pf} = -\bar{\eta}\sigma_0 - \bar{\mu}q_0$$

(22)

In the above equation, the expressions for α_1^2, $\bar{\eta}$ and $\bar{\mu}$ are similar to those of α^2, η and μ, respectively. But these are to be derived by considering $C_{ij}^f = C_{ij}^m = C_{ij}^p$. Solutions of Eqs. (21) and (22) are given by:

$$\bar{\sigma}_x^f = c_1 e^{\alpha x} + c_2 e^{-\alpha x} + \frac{\eta}{\alpha^2}\sigma + \frac{\mu}{\alpha^2}q$$

(23)

$$\bar{\sigma}_x^{pf} = c_3 e^{\alpha x} + c_4 e^{-\alpha x} + \frac{\bar{\eta}}{\alpha_1^2}\sigma_0 + \frac{\bar{\mu}}{\alpha_1^2}q_0$$

(24)

in which $\mathbf{c}_1$, $\mathbf{c}_2$, $\mathbf{c}_3$ and $\mathbf{c}_4$ are the constants of integrations to be evaluated from the following end conditions:

$$\bar{\sigma}_x^{pf} = \sigma_0 \text{ at } x = \pm L \text{ and } \bar{\sigma}_x^{f} = \bar{\sigma}_x^{pf} \text{ at } x = \pm L_f$$

(25)

Utilizing the end conditions given by (25) in Eqs. (23) and (24), the final solutions for $\bar{\sigma}_x^{pf}$ and $\bar{\sigma}_x^{f}$ are obtained as follows:

$$\bar{\sigma}_x^{pf} = \left\{ \frac{\cosh(\alpha_1 x)}{\cosh(\alpha_1 L)} \left(1 - \frac{\bar{\eta}}{\alpha_1^2} - \frac{\bar{\mu} q_0}{\alpha_1^2 \sigma_0} \right) + \frac{\bar{\eta}}{\alpha_1^2} + \frac{\bar{\mu}}{\alpha_1^2} \frac{q_0}{\sigma_0} \right\} \sigma_0$$

(26)

$$\bar{\sigma}_x^{f} = \left[\frac{\cosh(\alpha x)}{\cosh(\alpha L_f)} \left\{ \frac{\cosh(\alpha_1 L_f)}{\cosh(\alpha_1 L)} \left(1 - \frac{\bar{\eta}}{\alpha_1^2} - \frac{\bar{\mu} q_0}{\alpha_1^2 \sigma_0} \right) + \frac{\bar{\eta}}{\alpha_1^2} - \frac{\eta}{\alpha^2} + \left(\frac{\bar{\mu}}{\alpha_1^2} - \frac{\mu}{\alpha^2} \right) \frac{q_0}{\sigma_0} \right\} + \frac{\eta}{\alpha^2} + \frac{\mu q_0}{\alpha^2 \sigma_0} \right] \sigma_0$$

(27)

In the case that the fiber and matrix are isotropic, and with $\mathbf{q}_0$=0, the above model reduces to that presented by Gao and Li[9] for a CNT reinforced polymer composite. Finally, substitution of Eq. (27) into Eq. (7) yields the expression for the interface shear stress as follows:

$$\tau_i = -\frac{a}{2} \left[\frac{\alpha \sinh(\alpha x)}{\cosh(\alpha L_f)} \left\{ \frac{\cosh(\alpha_1 L_f)}{\cosh(\alpha_1 L)} \left(1 - \frac{\bar{\eta}}{\alpha_1^2} - \frac{\bar{\mu} q_0}{\alpha_1^2 \sigma_0} \right) + \frac{\bar{\eta}}{\alpha_1^2} - \frac{\eta}{\alpha^2} + \left(\frac{\bar{\mu}}{\alpha_1^2} - \frac{\mu}{\alpha^2} \right) \frac{q_0}{\sigma_0} \right\} \right] \sigma_0$$

(28)

3. Results and Discussion

The elastic coefficients of arm chair type **CNT**s with respect to the coordinate system considered here are obtained from Shen and Li[5] which are listed in Table 1. The polymer material and the carbon fiber are elastically isotropic. The isotropic elastic coefficients ($\mathbf{C_{ij}^p}$) of the polymer materia[18] and the elastic constants ($\mathbf{C_{ij}^f}$) of the high modulus M40 carbon fiber[34] needed for computing the numerical results are as given by

$$\mathbf{C_{11}^p = 5.3GPa},\ \mathbf{C_{12}^p = 3.1GPa},\ \mathbf{C_{11}^f = 373.89GPa}\ \text{and}\ \mathbf{C_{12}^f = 6.5GPa}.$$

A discussion on the effective properties of the **PNC** matrix is now in order. Recently, Ray and Batra[18] derived a micromechanics model to predict the effective properties of **CNT** and piezoelectric fiber reinforced hybrid composite. In the absence of piezoelectric fibers this micromechanics model is reduced to a model which predicts the effective elastic properties of the transversely isotropic **PNC** matrix with radially aligned **CNT**s considered here and is given by:

$$\mathbf{[C^m] = [C_1][V_3]^{-1} + [C_2][V_4]^{-1}} \tag{29}$$

The various matrices appearing in (29) are presented in the **Appendix**. At a particular value of **CNT** volume fraction ($\mathbf{V_{CNT}}$=1.0%), the effective values of the elastic constants $\mathbf{C_{ij}^m}$ of the **PNC** matrix predicted from Eq. (29) are presented in Table 2 for different types of armchair **CNT**s. Also, for $\mathbf{V_{CNT}}$=1.0%, the elastic constants $\mathbf{C_{ij}^m}$ of the **PNC**

matrix with (10, 10) **CNT**s presented in Table 2 yield the values of the Young's modulus ($\mathbf{E_r^m}$) in the radial direction and the Poisson's ratio ($\boldsymbol{\upsilon_{xr}^m}$) as 14.34 **GPa** and 0.369, respectively. The values of the same are also predicted identically from simple rule of mixtures validating the micromechanics model given by Eq. (29). Thus Eq. (29) can be used to compute the effective elastic constants $\mathbf{C_{ij}^m}$ of the **PNC** matrix for evaluating the numerical results.

For presenting the results, following nondimensional parameters are adopted:

$$\boldsymbol{\sigma^* = \frac{\bar{\sigma}_x^f}{\sigma_0}} \text{ and } \boldsymbol{\tau^* = \frac{10\tau_i}{\sigma_0}} \tag{31}$$

Unless otherwise mentioned, the values of the geometrical parameters of the **RVE** are taken as:

$$\mathbf{a = 3.5\mu m},\ \mathbf{R = a + 10\mu m},\ \mathbf{L_f / a = 10} \text{ and } \mathbf{L / L_f = 1.2}$$

Arm chair type (10, 10) CNTs are used to compute the numerical results for the axial stress and the interface shear stress, unless specifically varied. In order to validate the model derived in the previous section, first the normalized average axial stress in the fiber without coated with **CNT**s and the interface shear stress are compared with those obtained by an existing model[9] as shown in Figure 4. For this comparison, the fiber is an arm chair (10, 10) **CNT** as considered in Ref.[9]. It may be noted that the good

agreement between the two sets of results have been obtained verifying the present model. The marginal differences observed may be attributed to the fact that the model in Ref.[9] did not consider the radial deformation, whereas in the present model radial deformations have been taken into account. Next, results are computed for carbon fibers coated with radially aligned **CNT**s.

The variations of the axial normal stress in the short carbon fiber and the transverse shear stress at the interface between the fiber and the **PNC** matrix along the length of the fiber are shown in Figure 5. It may be observed that the carbon fiber coated with radially aligned-**CNT**s shares less load than the fiber without coated with **CNT**s. This is attributed simply to the radial and axial stiffening of the polymer matrix by the **CNT**s. Note that the axial Young's moduli of the **PNC** matrix with 1% (10, 10) **CNT** and the polymer are $\mathbf{E_x^m = 3.41 GPa}$ and $\mathbf{E_x^p = 3.01 GPa}$, respectively while the radial Young's moduli are $\mathbf{E_r^m = 14.34 GPa}$ and $\mathbf{E_r^p = 3.01 GPa}$, respectively. The **CNT**s create a radially orthotropic **PNC** matrix and an increase in the CNT volume fraction increases both the axial and radial modulii. Importantly, the maximum interfacial shear stress is reduced in the case of **CNT**s reinforcing the matrix. A critical parameter in the design of polymer matrices for composites is the ratio of this maximum stress to the strength of the matrix. Load sharing improves this ratio with the presence of only 1% **CNT**s by 23%, and it is also expected that the strength of the interface should increase due to the **CNT**s as well, further improving the effect. The axial load transferred to the carbon fiber and the interfacial shear stress decreases with the increase in the radial stiffness of the **PNC** matrix as shown in Figure 6 and Figure 7, respectively. Also, compared in Figure 6 and Figure 7is the case where the matrix remains isotropic but the value of its Young's

modulus is increased to that of $\mathbf{E_r^m}$ of the **PNC** with $\mathbf{V_{CNT}}$=1.0% (Poisson's ratio is assumed as 0.33). It may be observed from these figures that isotropically stiffening the matrix causes (as expected) a significant increase in load carried by the matrix and a reduction in the interfacial maximum shear stress beyond what is seen at 1% radially-aligned **PNC**.

In Figure 8, it may be seen that if the value of $(\mathbf{R/a})$ decreases then the load transfer from the matrix to the fiber coated with radially aligned CNTs significantly decreases as expected due to the larger proportion of overall load carried by the enhanced-stiffness matrix relative to the fiber. Beyond a few percent volume fraction of CNTs in the matrix, overall load sharing is not signficantly affected as evidenced both in Figure 8 and Figure 9. In Figure 9 the effect of **CNT** volume fraction on the critical length ($\mathbf{L_{crit}}$) of the fiber is presented. Here, $\mathbf{L_{crit}}$ is measured from the center of the fiber and determined based on the situation when $\sigma^* = 98\%$ of the maximum value of σ^*. It may be noted from this figure that as the **CNT** volume fraction increases, the critical length of the fiber decreases rapidly in the region $\mathbf{V_{CNT}} < 1.0\%$ and then decreases monotonically. For a particular value of volume fraction of the carbon fiber, the critical length increases if the aspect ratio of the fiber increases, while for a particular value of aspect ratio of the fiber this critical length decreases with the increase in the volume fraction of the carbon fiber. In Figure 10 a critical value of $\mathbf{V_{CNT}}$ is shown to exist beyond which the radial orthotropy of the **PNC** matrix does not appreciably alter load sharing capability of the fiber. After ~2% $\mathbf{V_{CNT}}$, there is little change in the load sharing between the **PNC** matrix and the fiber.

Variations of maximum values of the axial stress in the carbon fiber coated with

radially aligned **CNT**s ($\mathbf{V_{CNT}}$ =1.0%) and the interface shear stress with the aspect ratio of the fiber are presented in Figure 11. The maximum value of the axial load shared by the fiber increases sharply with the increase in the value of the aspect ratio as long as $\mathbf{L_f / a} < 12$. For $\mathbf{L_f / a} > 20$, the axial load sharing capability of the fiber becomes independent of the variation of the aspect ratio of the fiber. In case of interface shear stress, its maximum value also increases rapidly with the increase in the value of the aspect ratio of the fiber till $\mathbf{L_f / a} < 8$. The maximum value of $\boldsymbol{\tau}^*$ becomes saturated for $\mathbf{L_f / a} > 10$.

The effect of application of radial load on the load transferred to the fiber is presented in Figure 12. If the applied radial load is compressive, then the maximum values of the axial normal stress in the fiber and the interface shear stress are higher than those without the application of radial load ($\mathbf{q}_0 = 0$), and vice versa. The variations of axial normal stress in the carbon fiber and the interface shear stress along its length are presented in Figure 13 and Figure 14, respectively, for different arm chair type **CNT**s in Table 1. It may be observed from these figures that for a particular value of $\mathbf{V_{CNT}}$, as the diameter of **CNT** increases, both the axial normal load transferred to the fiber and the interface shear stress increase. This may be attributed to the fact that as the diameter of **CNT** increases, elastic coefficients of **CNT** decreases (see Table 1) which results in the decrease in the values of the effective elastic properties of the **CNT**-reinforced **PNC** matrix. Overall, the type of **CNT** has a small effect on the composite fiber load sharing relative to varying volume fraction of the **CNT**s in the **PNC** matrix.

4. Conclusions

In this paper, load sharing in a shortfiber composite where the matrix is reinforced with radially-aligned **CNT**s has been analyzed. The fiber reinforcement of the composite is a discontinuous carbon fiber coated with radially aligned **CNT**s. A shear lag model considering radial and axial deformations of the different phases of the **RVE** has been developed to analyze the axial load transferred to this carbon fiber. Since the radially aligned **CNT**s grown on the carbon fiber reinforce the polymer matrix, the effective elastic properties of the resulting **CNT**-reinforced **PNC** matrix are modified. Hence, if the fiber is coated with **CNT**s, the axial load transferred to the carbon fiber and the shear stress at the interface between the fiber and the **PNC** matrix decrease, and the **CNT**-reinforced matrix carries more of this load. If the volume fraction of **CNT**s increases, both the axial load transferred to the fiber and the interface shear stress decrease, including importantly the maximum shear stress at the fiber-matrix interface. The critical length of the carbon fiber varies little with **CNT** volume fraction beyond a few percent. For a particular value of **CNT** volume fraction, compressive radial load applied to the **RVE** increases the axial load transferred to the fiber and the interface shear stress. Future work should consider load-transfer in randomly-oriented shortfiber composites, and also load transfer around a broken fiber in continuous filament composites, in addition to load sharing in the presence of applied shear stress.

Appendix

The various matrices appearing in Eq. (29) are given by

$$[\mathbf{C}_1]=\mathbf{v_n}\begin{bmatrix}0&0&0&0&0&0\\0&0&0&0&0&0\\\mathbf{C}^{\mathbf{n}}_{13}&\mathbf{C}^{\mathbf{n}}_{23}&\mathbf{C}^{\mathbf{n}}_{33}&0&0&0\\0&0&0&0&0&0\\0&0&0&0&0&0\\0&0&0&0&0&0\end{bmatrix},\ [\mathbf{C}_2]=\begin{bmatrix}\mathbf{C}^{\mathbf{p}}_{11}&\mathbf{C}^{\mathbf{p}}_{12}&\mathbf{C}^{\mathbf{p}}_{12}&0&0&0\\\mathbf{C}^{\mathbf{p}}_{12}&\mathbf{C}^{\mathbf{p}}_{11}&\mathbf{C}^{\mathbf{p}}_{12}&0&0&0\\\mathbf{v_p}\mathbf{C}^{\mathbf{p}}_{12}&\mathbf{v_p}\mathbf{C}^{\mathbf{p}}_{12}&\mathbf{v_p}\mathbf{C}^{\mathbf{p}}_{11}&0&0&0\\0&0&0&\mathbf{C}^{\mathbf{p}}_{44}&0&0\\0&0&0&0&\mathbf{C}^{\mathbf{p}}_{44}&0\\0&0&0&0&0&\mathbf{C}^{\mathbf{p}}_{44}\end{bmatrix},$$

$$\mathbf{v_n}=\frac{\mathbf{R}^2}{\mathbf{R}^2-\mathbf{a}^2}\mathbf{V_{CNT}},\ \mathbf{v_p}=1-\mathbf{v_n},\ [\mathbf{V}_3]=[\mathbf{V}_1]+[\mathbf{V}_2][\mathbf{C}_4]^{-1}[\mathbf{C}_3],\ [\mathbf{V}_4]=[\mathbf{V}_2]+[\mathbf{V}_1][\mathbf{C}_3]^{-1}[\mathbf{C}_4],$$

$$[\mathbf{C}_3]=\begin{bmatrix}\mathbf{C}^{\mathbf{n}}_{11}&\mathbf{C}^{\mathbf{n}}_{12}&\mathbf{C}^{\mathbf{n}}_{13}&0&0&0\\\mathbf{C}^{\mathbf{n}}_{12}&\mathbf{C}^{\mathbf{n}}_{22}&\mathbf{C}^{\mathbf{n}}_{23}&0&0&0\\0&0&1&0&0&0\\0&0&0&\mathbf{C}^{\mathbf{n}}_{44}&0&0\\0&0&0&0&\mathbf{C}^{\mathbf{n}}_{55}&0\\0&0&0&0&0&\mathbf{C}^{\mathbf{n}}_{66}\end{bmatrix},\ [\mathbf{C}_4]=\begin{bmatrix}\mathbf{C}^{\mathbf{p}}_{11}&\mathbf{C}^{\mathbf{p}}_{12}&\mathbf{C}^{\mathbf{p}}_{12}&0&0&0\\\mathbf{C}^{\mathbf{p}}_{12}&\mathbf{C}^{\mathbf{p}}_{11}&\mathbf{C}^{\mathbf{p}}_{12}&0&0&0\\0&0&1&0&0&0\\0&0&0&\mathbf{C}^{\mathbf{p}}_{44}&0&0\\0&0&0&0&\mathbf{C}^{\mathbf{p}}_{44}&0\\0&0&0&0&0&\mathbf{C}^{\mathbf{p}}_{44}\end{bmatrix},$$

$$[\mathbf{V}_1]=\begin{bmatrix}\mathbf{v_n}&0&0&0&0&0\\0&\mathbf{v_n}&0&0&0&0\\0&0&0&0&0&0\\0&0&0&\mathbf{v_n}&0&0\\0&0&0&0&\mathbf{v_n}&0\\0&0&0&0&0&\mathbf{v_n}\end{bmatrix}\text{ and }[\mathbf{V}_2]=\begin{bmatrix}\mathbf{v_p}&0&0&0&0&0\\0&\mathbf{v_p}&0&0&0&0\\0&0&1&0&0&0\\0&0&0&\mathbf{v_p}&0&0\\0&0&0&0&\mathbf{v_p}&0\\0&0&0&0&0&\mathbf{v_p}\end{bmatrix}$$

(2)

In the above matrices, $\mathbf{C_{ij}^{n}}$ and $\mathbf{C_{ij}^{p}}$ are the elastic coefficients of the **CNT** and the polymer material, respectively. The volume fractions of the polymer and the **CNT** with respect to the volume of the **PNC** are represented by $\mathbf{v_p}$ and $\mathbf{v_n}$ while $\mathbf{V_{CNT}}$ denotes the volume fraction of **CNT**s with respect to the volume of the **RVE**.

References

[1]S. Iijima, Helical microtubules of graphitic carbon, *Nature* **1991**, *354*, 56-58.

[2]M. M. J. Treacy, T. W. Ebbessen, J. M. Gibson, Exceptionally high Young's modulus observed for individual carbon nanotubes, *Nature* **1996**, *381*, 678 - 680.

[3]C. Li, T. W. Chou, A structural mechanics approach for the analysis of carbon nanotubes, *International Journal of Solids Structures* **2003**, *40*, 2487 - 2499.

[4]A. Sears, R. C. Batra, Macroscopic properties of carbon nanotubes from molecular mechanics simulations, *Physical Review B* **2004**, *69*, 1-10.

[5]L. Shen, J. Li, Transversely isotropic elastic properties of single-walled carbon nanotubes, *Physical Review B* **2004**, *69*, 1-10.

[6]R. C. Batra, A. Sears, Uniform radial expansion/contraction of carbon nanotubes and their transverse elastic moduli, *Modelling and Simulation in Materials Science and Engineering* **2007**, *15*, 835-844.

[7]J. Wu, K. C. Hwang, Y. Huang, An atomistic-based finite-deformation shell theory for single-wall carbon nanotubes, *Journal of the Mechanics and Physics of Solids* **2008**, *56*, 279-292.

[8]E. T. Thostenson, T. W. Chou, On the elastic properties of carbon nanotube based composites: modeling and characterization, *Journal of Physics D: Applied Physics* **2003**, *36*, 573-582.

[9]X. L. Gao, K. Li, A shear-lag model for carbon nanotube reinforced polymer composites, *International Journal of Solids and Structures* **2005**, *42*, 1649-1667.

[10]Y. S. Song, J. R. Youn, Modeling of effective elastic properties for polymer based carbon nanotube composites, *Polymer* **2006**, *47*, 1741-1748.

[11]G. D. Seidel, D. C. Lagoudas, Micromechanical analysis of the effective elastic properties of carbon nanotube reinforced composites, *Mechanics of materials* **2006**, *38*, 884-907.

[12]R. Guzman de Villoria, A. Miravete, Mechanical model to evaluate the effect of the dispersion in nanocomposites, *Acta Materialia* **2007**, *55*, 3025-3031.

[13]L. Y. Jiang, H. L. Tan, J. Wu, Y. G. Huang, K. C. Hwang, Continuum modeling of interfaces in polymer matrix composites reinforced by carbon nanotubes, *Nano Letters* **2007**, *2*, 139-148.

[14]G. M. Odegard, T. S. Gates, K. E. Wise, C. Park, E. J. Siochi, Constitutive modeling of nanotube-reinforced polymer composites, *Composites Science and Technology* **2003**, *63*, 1671-1687.

[15]G. M. Odegard, T. S. Gates, L. M. Nicholson, K. E. Wise, Equivalent-Continuum Modeling of Nano-Structured Materials, *Composites Science and Technology* **2002**, *62*, 1869-1880.

[16]V. I. Yamakov, E. H. Glaessegen, To twin or not to twin, *Nature Materials* **2007**, *6*, 795-796.

[17]J. Zhang, C. He, A three-phase cylindrical shear-lag model for carbon nanotube composites, *Acta Mechanica* **2008**, *196*, 33-54.

[18]M. C. Ray, R. C. Batra, Effective properties of carbon nanotube and piezoelectric fiber reinforced hybrid smart composite, *accepted in ASME Journal of Applied mechanics* **2008**.

[19]E. T. Thostenson, C. Li, T.-W. Chou, Nanocomposites in context, *Composites Science and Technology* **2005**, *65*, 491-516.

[20]E. T. Thostenson, Z. Ren, T.-W. Chou, Advances in the science and technology of carbon nanotubes and their composites: a review, *Composites Science and Technology* **2001**, *61*, 1899-1912.

[21]J. N. Coleman, U. Khan, W. J. Blau, Y. K. Gun'ko, Small but strong: A review of the mechanical properties of carbon nanotube-polymer composites, *Carbon* **2006**, *44*, 1624-1652.

[22]J. O. Zhao, L. Liu, Q. G. Guo, J. Shi , G. Zhai , J. Song, Z. Liu, Growth of carbon nanotubes on the surface of carbon fibers, *Carbon* **2008**, *46*, 380-383.

[23]Q. J. Gong, H. J. Li, X. Wang, Q. G. Fua, Z. W. Wanga, K. Z. Lia, In situ catalytic growth of carbon nanotubes on the surface of carbon cloth, *Composite Science and Technology* **2007**, *67*, 2986-2989.

[24]L. T. Qu, Y. Zhao, L. M. Dai, Carbon microfibers sheathed with aligned carbon nanotubes: Towards multidimensional, multicomponent, and multifunctional nanomaterials, *Small* **2006**, *2*, 1052-1059.

[25]L. J. Ci, Z. G. Zhao, J. B. Bai, Direct growth of carbon nanotubes on the surface of ceramic fibers, *Carbon* **2005**, *43*, 883-886.

[26]Z. G. Zhao, L. J. Ci, H. M. Cheng, J. B. Bai, The growth of multi-walled carbon nanotubes with different morphologies on carbon fibers, *Carbon* **2005**, *43*, 663-665.

[27]R. B. Mathur, S. Chatterjee, B. P. Singh, Growth of carbon nanotubes on carbon fibre substrates to produce hybrid/phenolic composites with improved mechanical properties, *Composite Science and Technology* **2008**, *68*, 1608-1615.

[28]V. P. Veedu, A. Cao, X. Li, K. Ma, C. Soldano, S. Kar, P. M. Ajayan, M. N. Ghasemi-Nejhad, Multifunctional Composites Using Reinforced Laminae with Carbon Nanotube Forests, *Nature Materials* **2006**, *5*, 457-462.

[29]E. J. Garcia, B. L. Wardle, A. J. Hart, N. Yamamoto, Fabrication and Multifunctional Properties of a Hybrid Laminate with Aligned Carbon Nanotubes Grown In Situ, *Composites Science & Technology* **2008**, *68*, 2034-2041.

[30]E. J. García, A. J. Hart, B. L. Wardle, A. H. Slocum, Fabrication of composite microstructures by capillarity-driven wetting of aligned carbon nanotubes with polymers, *Nanotechnology* **2007**, *18*, 165602 (165611 pp).

[31]K. I. Winey, R. A. Vaia, Polymer Nanocomposites, *MRS Bulletin* **2007**, *32*, 314-322.

[32]P. Ajayan, P. Braun, L. Schadler, *Nanocomposite Science and Technology*, **2003**.

[33]Z. Hashin, W. Rosen, The elastic moduli of fiber reinforced materials, *Journal of Applied Mechanics* **1964**, *31*, 223-232.

[34]J. D. H. Hughes, The carbon fiber/epoxy interface - a review, *Composite Science and Technology* **1991**, *41*, 13-45.

List of tables

Table 1. Material properties of CNTs (Ref. 5). The 3-axis is aligned with the long axis of the CNT.

CNT Type	$\mathbf{C}_{11}^{\mathbf{n}}$ (GPa)	$\mathbf{C}_{22}^{\mathbf{n}}$ (GPa)	$\mathbf{C}_{33}^{\mathbf{n}}$ (GPa)	$\mathbf{C}_{12}^{\mathbf{n}}$ (GPa)	$\mathbf{C}_{13}^{\mathbf{n}}$ (GPa)	$\mathbf{C}_{44}^{\mathbf{n}}$ (GPa)	$\mathbf{C}_{55}^{\mathbf{n}}$ (GPa)	$\mathbf{C}_{66}^{\mathbf{n}}$ (GPa)
(5,5)	668	668	2143	404	184	791	791	132
(10,10)	288	288	1088	254	87.7	442	442	17
(20,20)	138	138	545	134	43.5	227	227	2
(50,50)	55.1	55.1	218	54.9	17.5	92	92	0.1

Table 2. Material properties of PNC with different arm chair type CNTs

($V_{CNT} = 1.0\%$).

PNC with **CNT** Type	C_{11}^m (GPa)	C_{22}^m (GPa)	C_{33}^m (GPa)	C_{12}^m (GPa)	C_{13}^m (GPa)	C_{44}^m (GPa)	C_{55}^m (GPa)	C_{66}^m (GPa)
(5,5)	5.357	5.357	27.565	3.133	3.115	1.112	1.112	1.112
(10,10)	5.356	5.356	16.628	3.134	3.114	1.112	1.112	1.112
(20,20)	5.349	5.349	10.956	3.139	3.114	1.112	1.112	1.112
(50,50)	5.235	5.235	7.546	3.248	3.111	1.112	1.112	1.112

List of figures

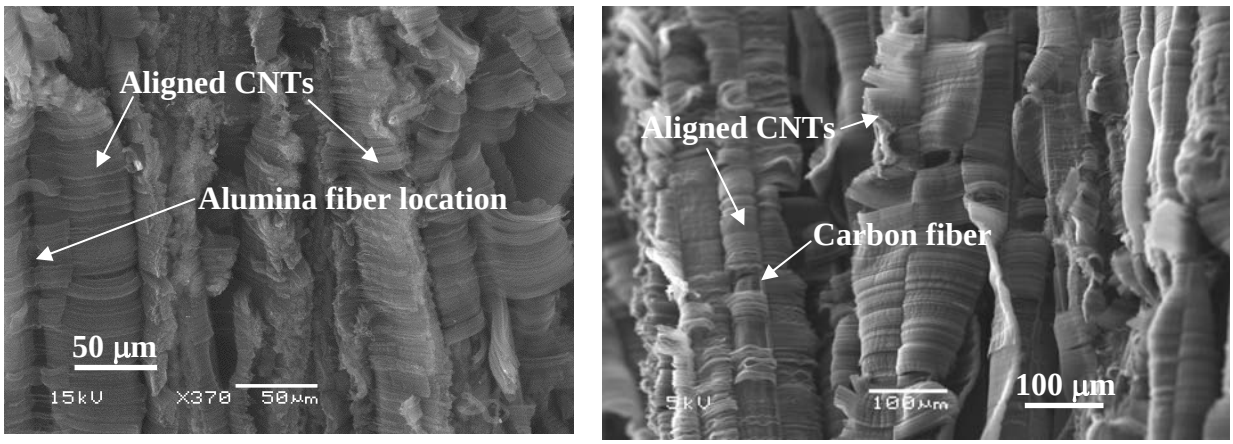

Figure 1. Fibers coated with in situ grown radially aligned CNTs. Fuzzy alumina (left) and carbon fiber (right).

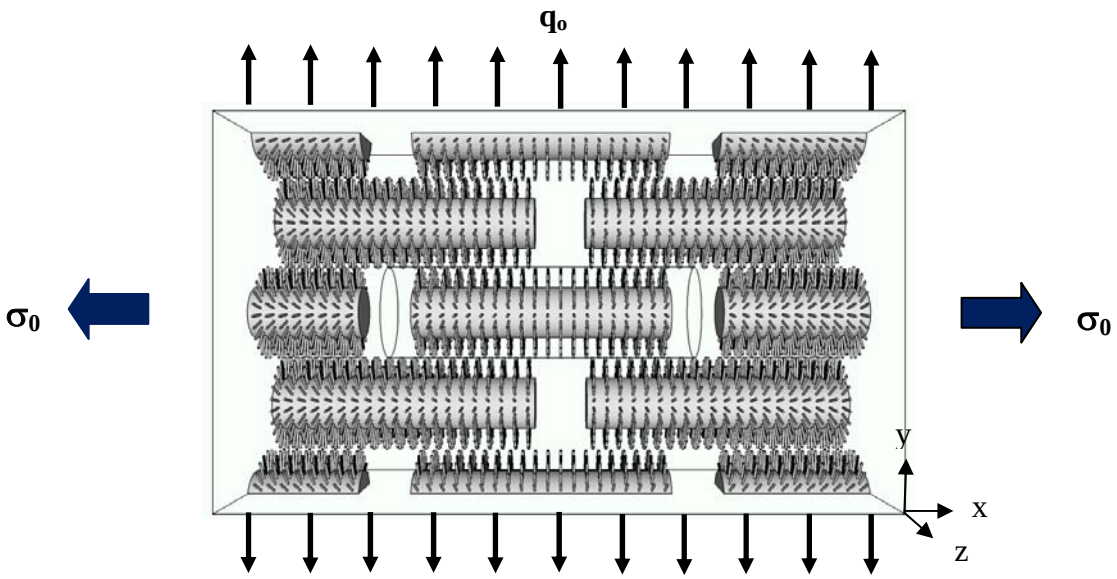

Figure 2. Model nano-engineered composite with representative volume element (RVE) indicated at the center.

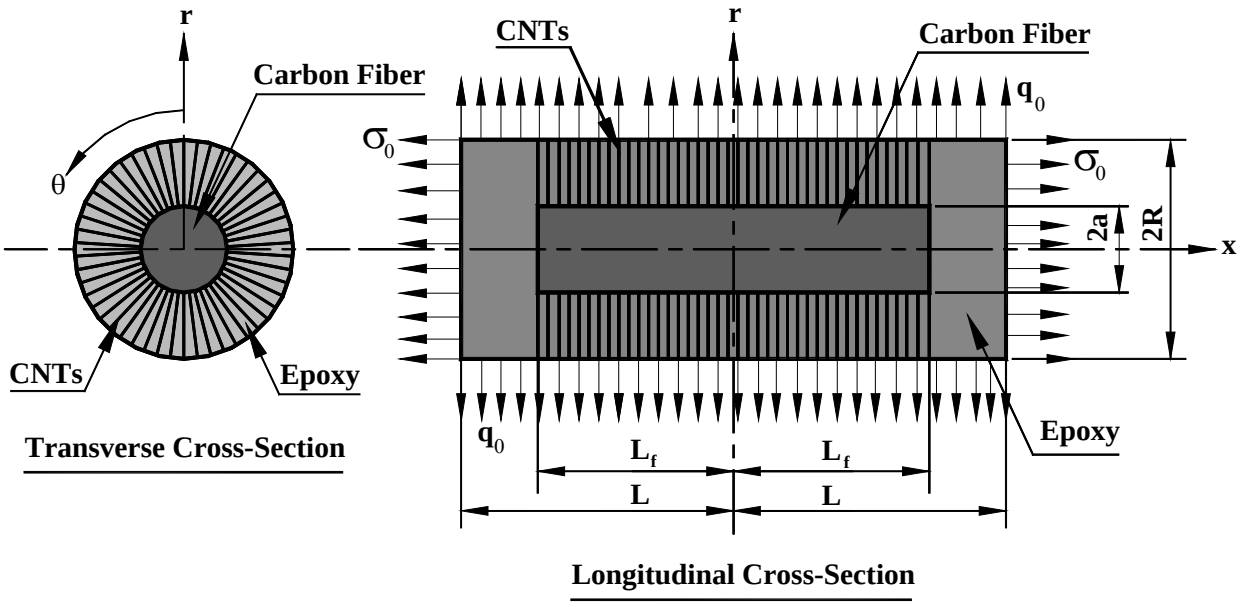

Figure 3. RVE of the composite containing a fiber reinforcement coated with radially-aligned CNTs.

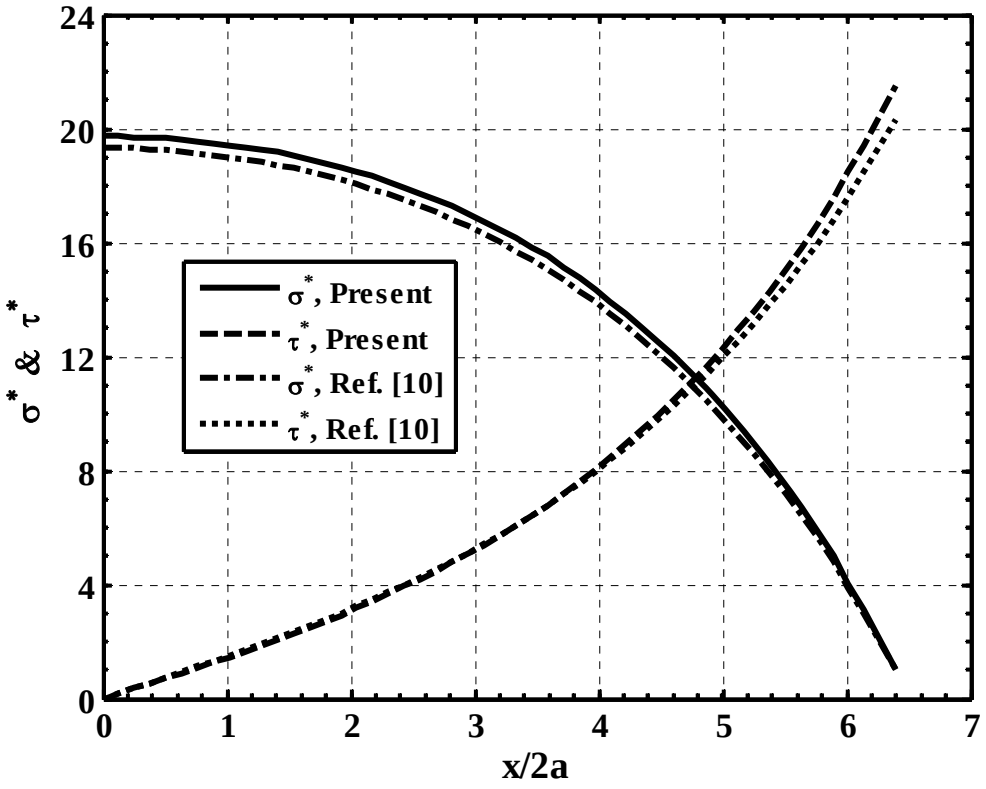

Figure 4. Model validation by comparison to Ref.[9] for the case of an isotropic matrix phase (no CNTs) around the fiber. $\mathbf{L_f}/\mathbf{a}$=10

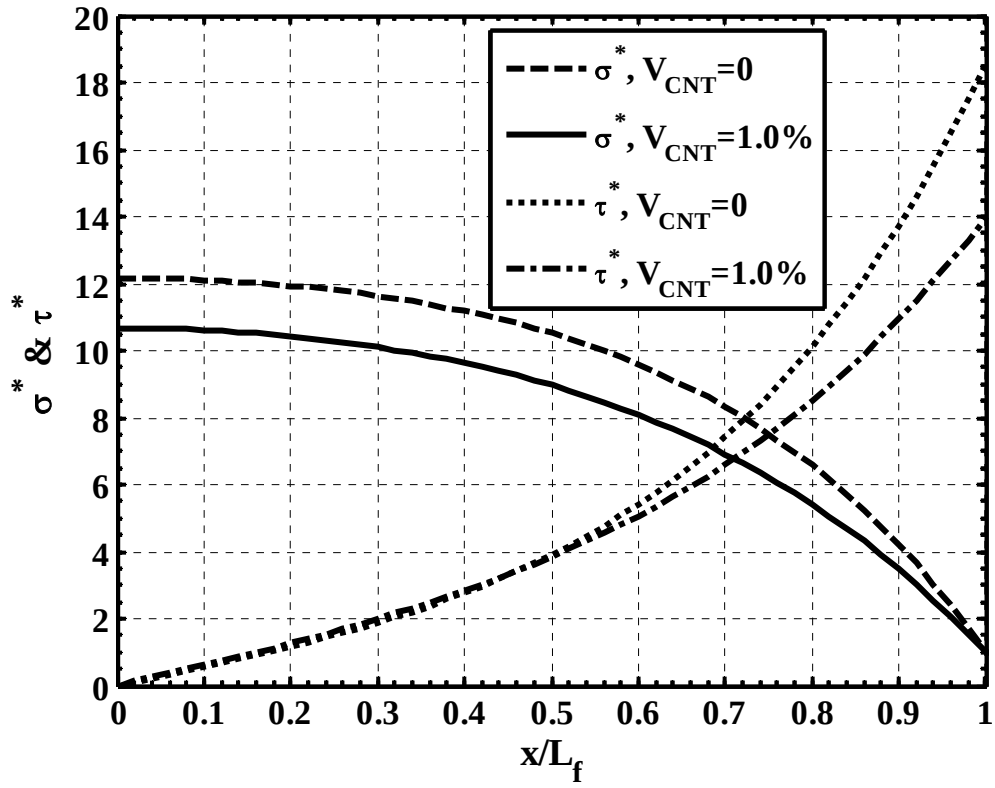

Figure 5. Variation of normalized axial normal stress in the carbon fiber and the interface shear stress along the fiber length ($\mathbf{q}_0 = 0$).

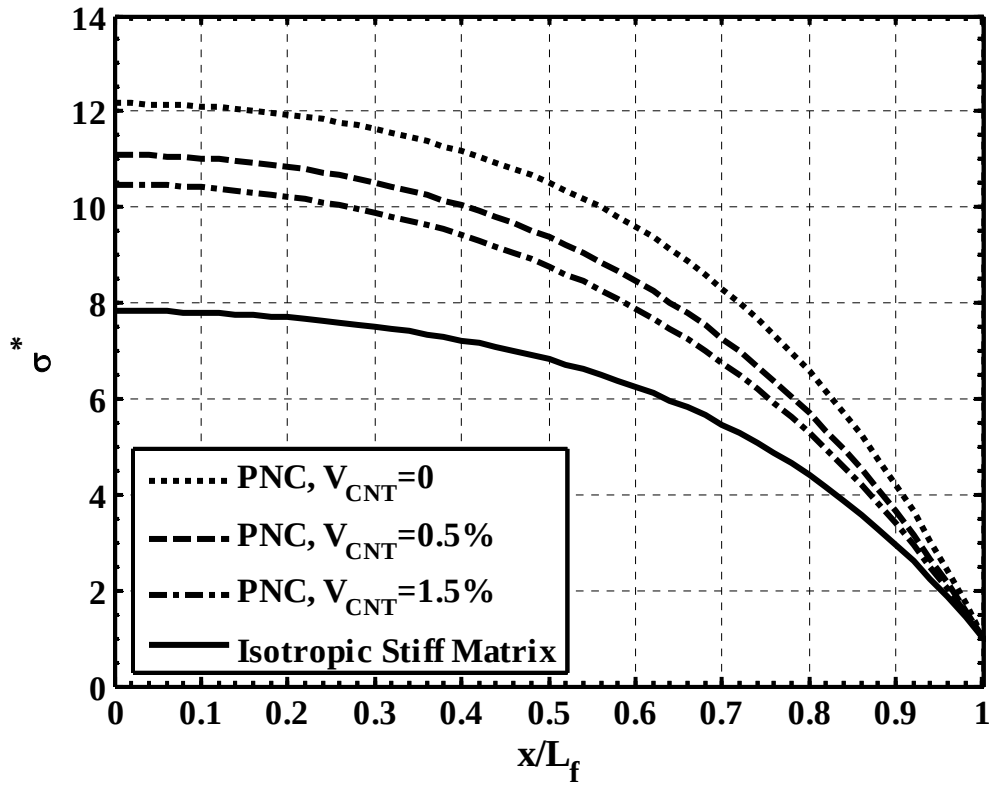

Figure 6. Variation of axial normal stress in the carbon fiber along its length

$(\mathbf{q}_0 = 0)$

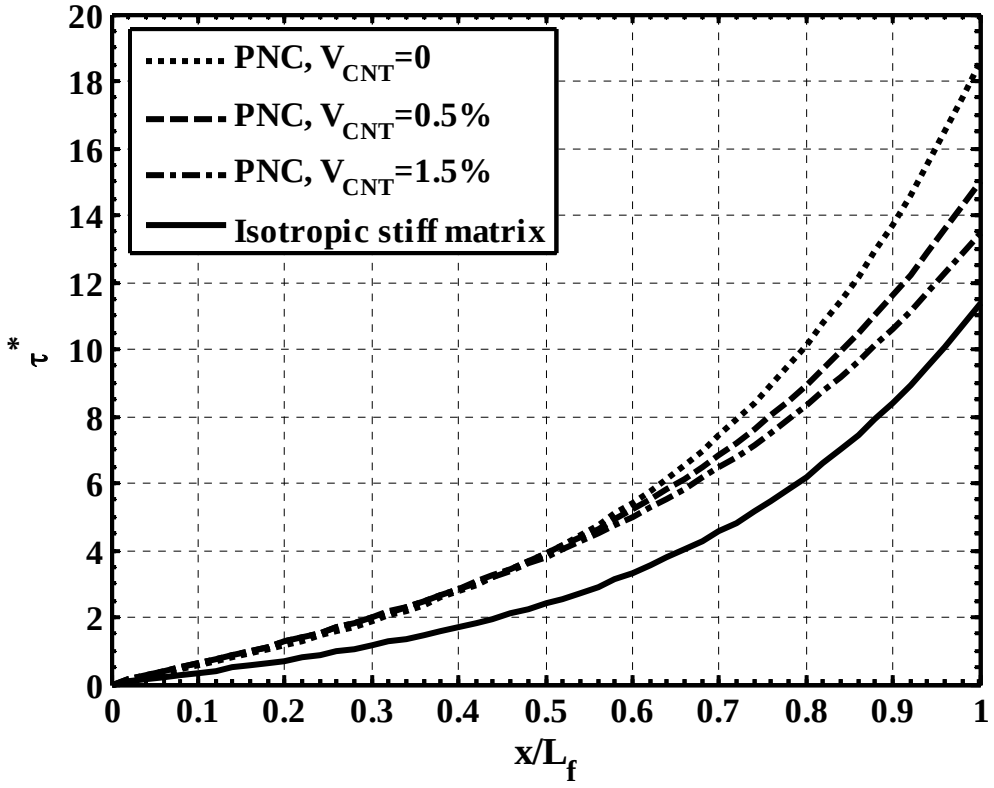

Figure 7. Variation of transverse shear stress at the interface between the matrix and the carbon fiber along the length of the fiber for different CNT volume fraction and considering isotropic stiffening of the matrix ($\mathbf{q}_0 = 0$).

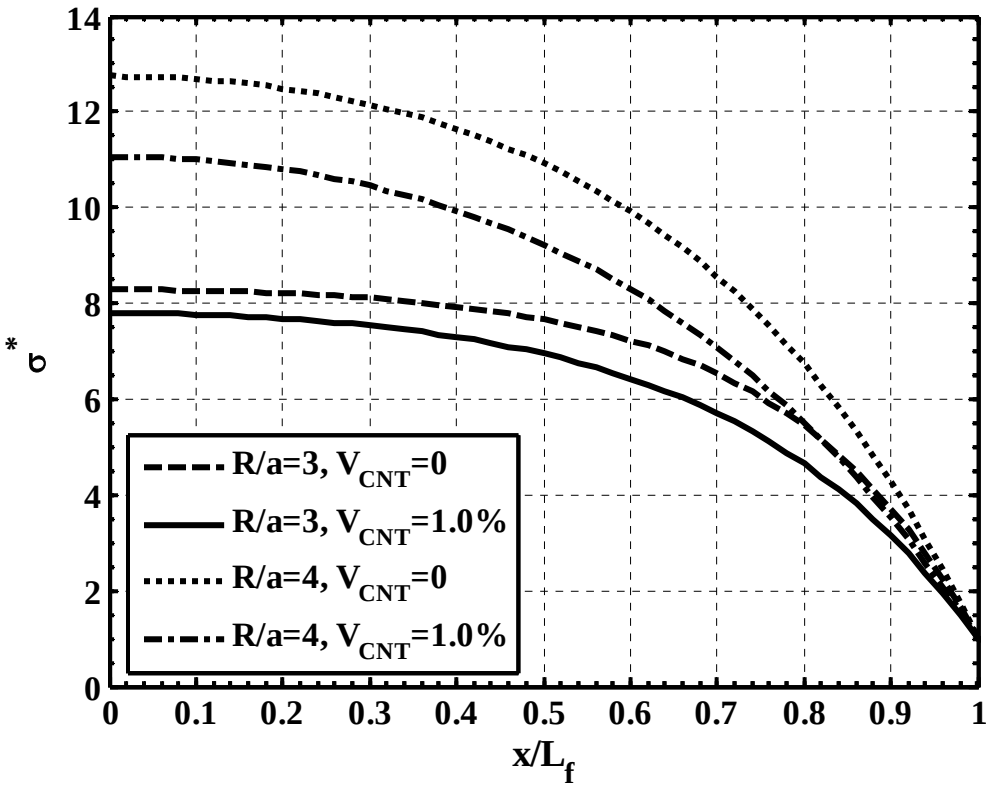

Figure 8. Load transfer in the carbon fiber for different values of $\mathbf{R/a}$ ($\mathbf{V_{CNT}} = 1.0\%$, $\mathbf{q}_0 = 0$)

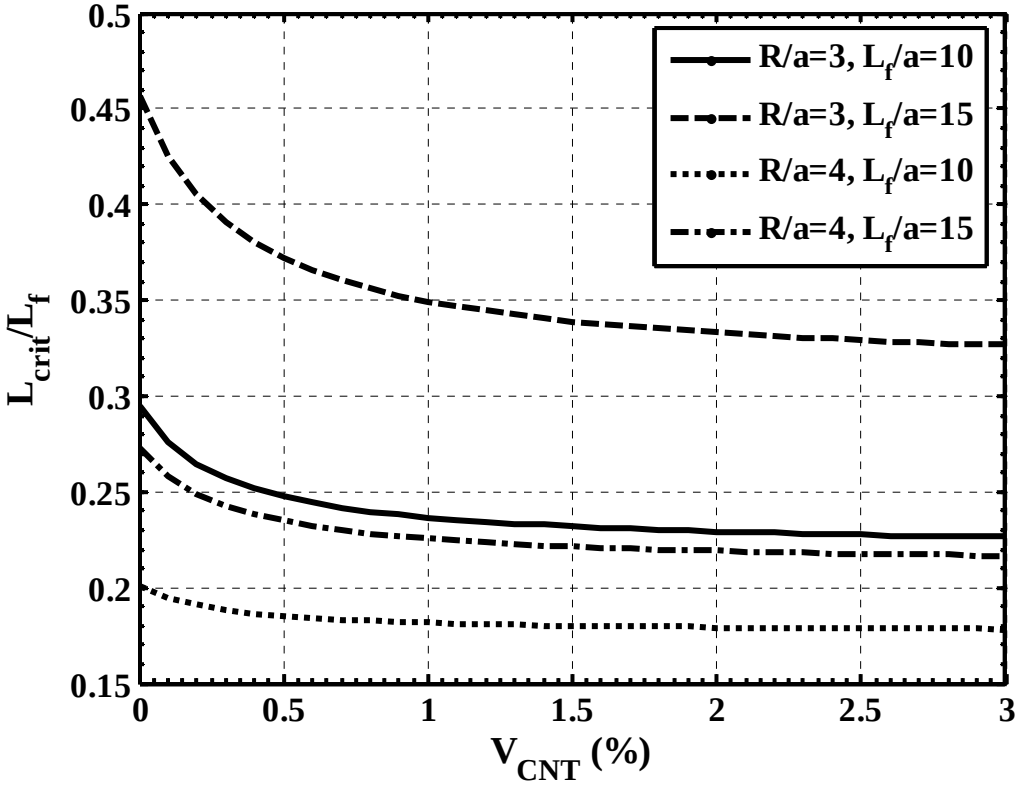

Figure 9. Effect of CNT volume fraction on the critical length of a fiber for full load transfer ($\mathbf{q}_0 = 0$).

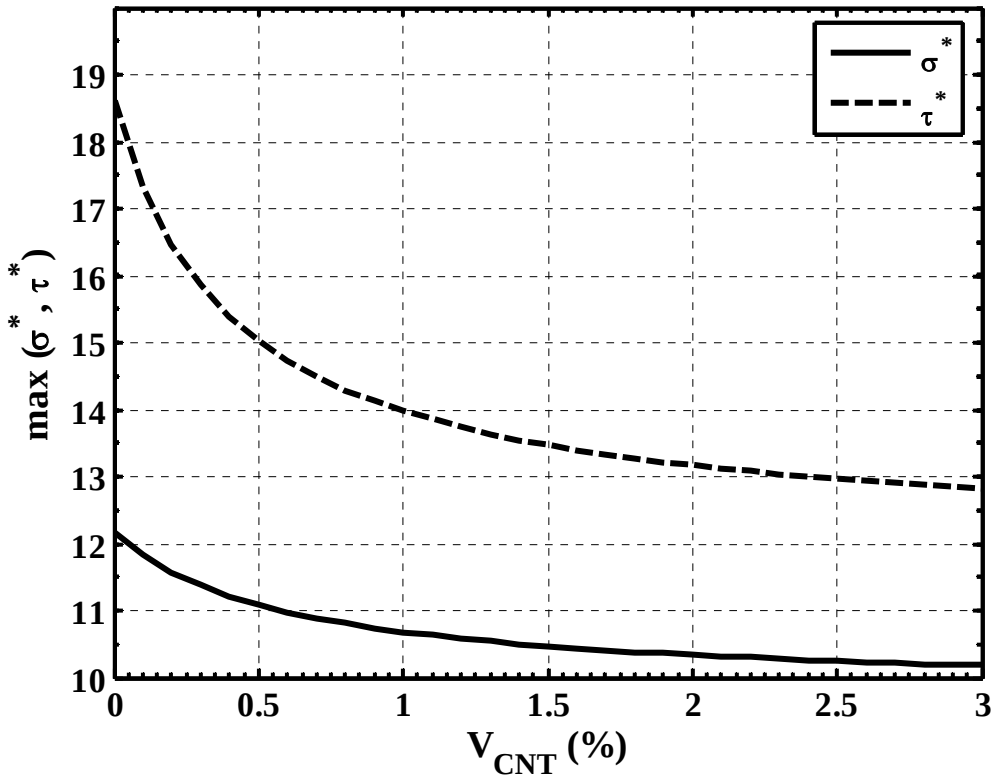

Figure 10. Variation of maximum axial stress and interfacial shear stress on the carbon fiber ($\mathbf{L\_f / a} = 10$) as a function of CNT volume fraction ($\mathbf{q}_0 = 0$).

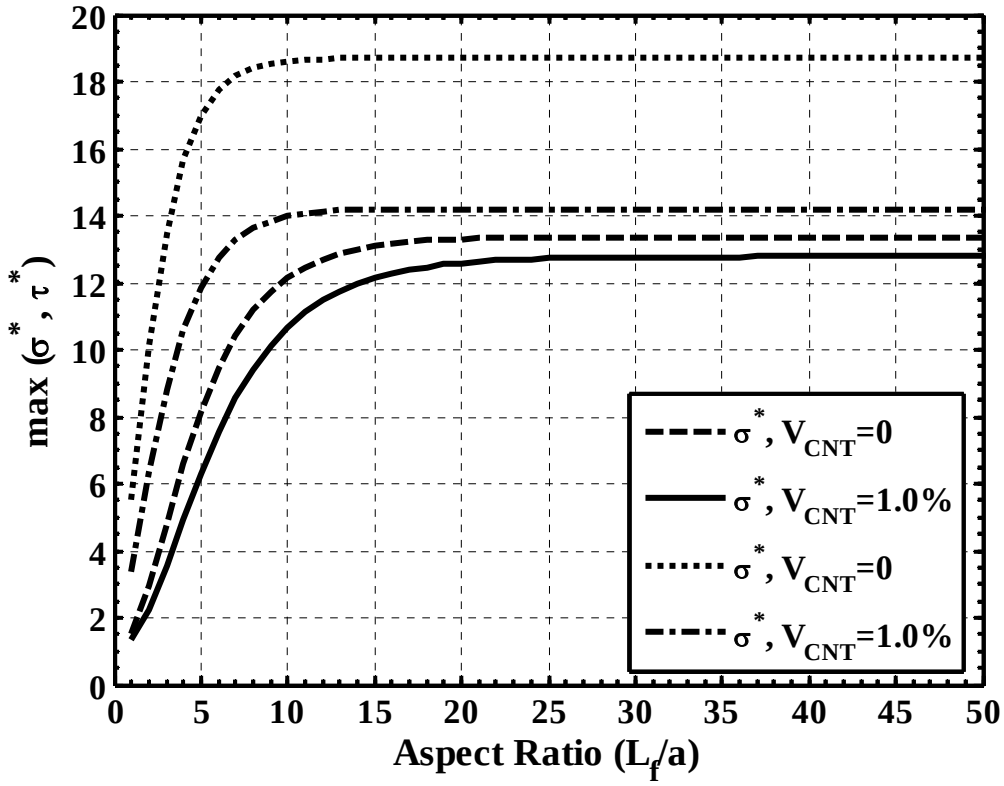

Figure 11. Variation of maximum values of the axial normal stress and the transverse shear stress at the interface between the matrix and the carbon fiber with the aspect ratio of the fiber ($\mathbf{q}_0 = 0$, $\mathbf{V_{CNT}} = 1.0\%$).

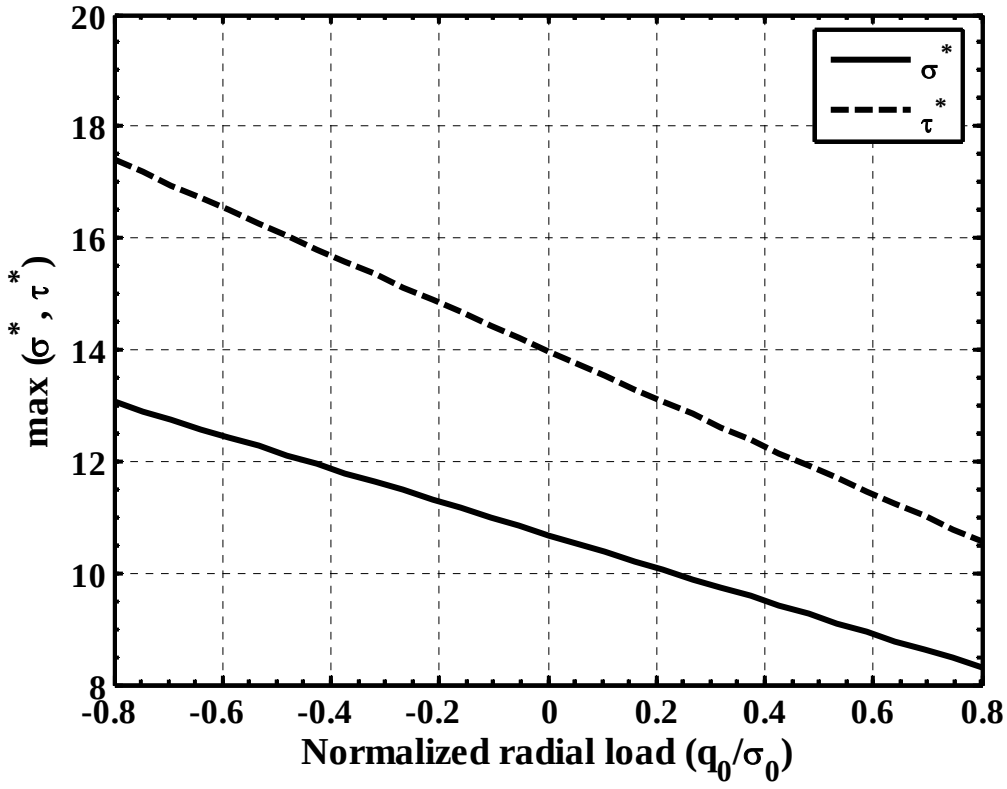

Figure 12. Variation of maximum values of the axial normal stress and the transverse shear stress at the interface between the matrix and the carbon fiber with the applied radial load ($\mathbf{L_f / a = 10}$, $\mathbf{V_{CNT} = 1.0\%}$).

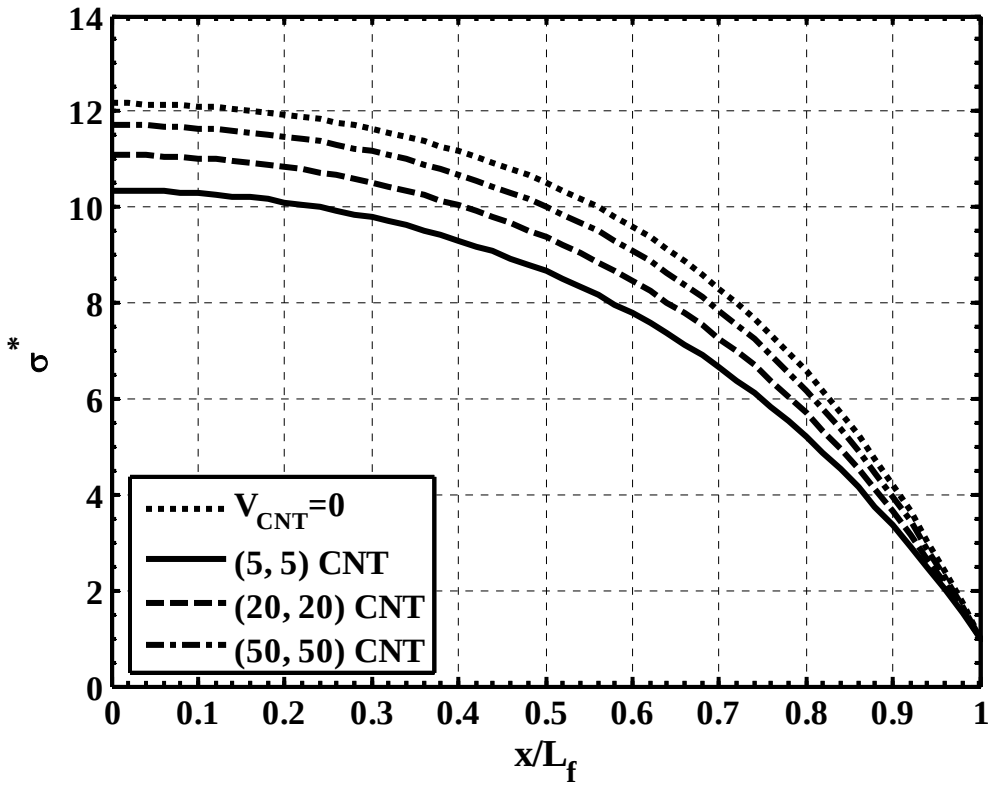

Figure 13. Variation of the axial normal stress in the carbon fiber along its length when the fiber is coated with different arm chair type CNTs ($\mathbf{q}_0 = 0$, $\mathbf{V}_{\mathbf{CNT}} = 1.0\%$).

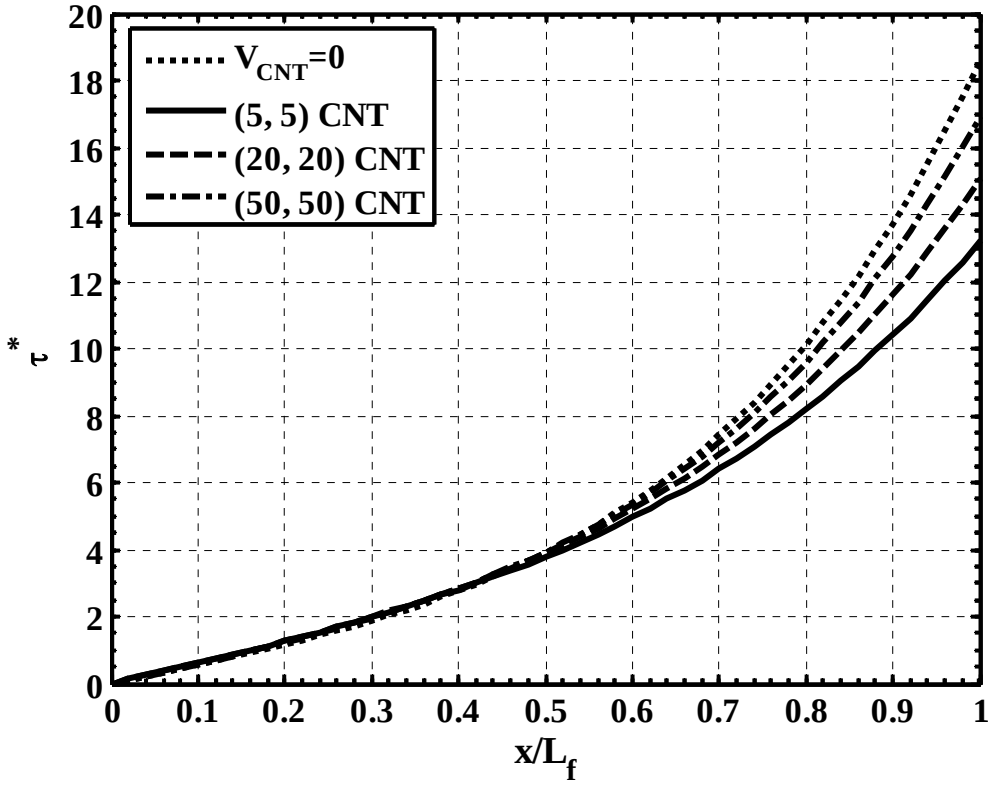

Figure 14. Variation of the transverse shear stress at the interface between the matrix and the carbon fiber along its length when the fiber is coated with different arm chair type CNTs ($\mathbf{q}_0 = 0$, $\mathbf{V_{CNT}} = 1.0\%$).